Science and Technology Infusion Climate Bulletin
NOAA's National Weather Service
40th NOAA Annual Climate Diagnostics and Prediction Workshop
Denver, CO, 26-29 October 2015

What Drove Tropical and North Pacific and North America Climate Anomalies in 2014/15 Winter?

Peitao Peng, Arun Kumar and Zeng-Zhen Hu
Climate Prediction Center, NOAA/NWS/NCEP, College Park, Maryland

1. Introduction

From October 2014 to March 2015, the Niño3.4 index, referred to as sea surface temperature (SST) anomaly averaged over 170°W-120°W, 5°S-5°N, was in a 0.5°C to 0.9°C range. At the same time, except for the February 2015, the southern oscillation index (SOI), defined as the standardized surface pressure difference between Tahiti and Darwin (former minus later), was in a range of -0.6 to -0.9. The values of the both indices exceeded the thresholds for a weak El Niño conditions (Trenberth 1998). However, the atmospheric anomalies over the same time did not reflect typical ENSO like conditions, leading to the question why atmospheric circulation did not show a response typical to what is generally observed during El Niño conditions?

To illustrate this point further, comparison of spatial pattern between the observed December-January-February 2014/15 seasonal mean (referred to as DJF 2014/15) and the Niño3.4 index based regression patterns for DJF mean SST, precipitation rate (Prate) and 200hPa stream function (S200) is shown in Fig. 1. The Niño3.4 index regression patterns represent the spatial patterns that are typically seen during ENSO winters.

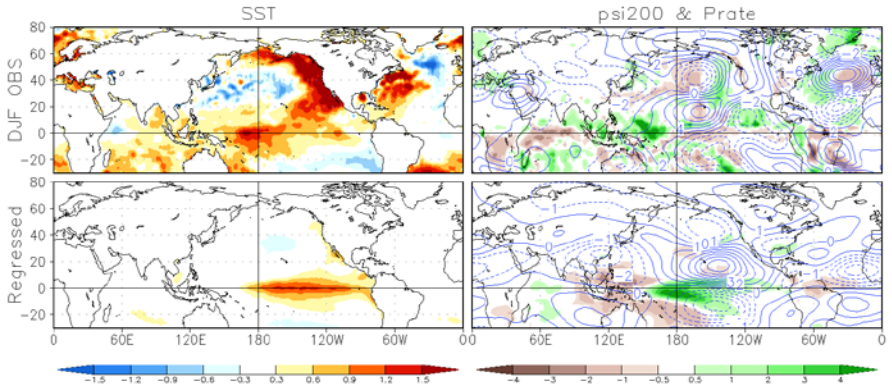

Fig. 1 Upper row: DJF mean SST (left), 200hPa stream function (contours in right) and precipitation rate (shadings in right) observed in the winter of 2014/15. Lower row: Regressions of SST, 200hPa stream function and precipitation rate onto Niño3.4 SST index for the data period (1949/50-2014/15 for SST and stream function, 1979/80-2014/15 for precipitation). Units: °C for SST, 10^6 m^2 s^{-1} for stream function and mm/day for precipitation rate.

For the Niño3.4 index regressed SST pattern (Fig. 1, bottom left), the largest anomalies are in the eastern to central equatorial Pacific, and further, are confined to the east of the date line. In contrast, the observed SST anomalies for DJF 2014/15 in the tropics had their warm center located over the central Pacific and even extended to the west of the dateline. Also, the warm SST anomalies in the tropics extended along a circular arch northeastward towards and along the western coast of North America.

For Prate, the Niño3.4 index regressed pattern (Fig. 1, bottom right) in the tropical latitudes is the familiar dipole pattern, with the positive anomalies extending from the eastern equatorial Pacific to the warm pool region and the negative anomalies covering the Maritime continent region and its vicinity, and extending over to the South Pacific convergence zone (SPCZ). The spatial pattern of Prate corresponds well with the SST pattern in both shape and sign, indicating a *forced* response to SST, a fact that has been validated earlier in atmospheric general circulation model simulations (Peng *et al.* 2014). The corresponding DJF 2014/15 observed Prate pattern is also an east-west dipole pattern, however, with a reversed polarity. The positive

Correspondence to: Peitao Peng, 5830 University Research Court, Climate Prediction Center, NOAA/NWS/NCEP, College Park, Maryland; E-mail: peitao.peng@noaa.gov

anomaly is in the western tropical Pacific and the maritime continent area, and the negative anomaly in the central equatorial Pacific. This contrast in Prate pattern between the observed and ENSO was noted by Barnston (2015).

Although the difference in Prate pattern is so striking, the observed and regression S200 patterns are surprisingly similar in the tropics. They both have an anti-cyclonic pair straddling the equator over the central Pacific. The difference between them is that the observed pattern is shifted westward about 15° with respect to the Niño3.4 index regression pattern. Furthermore, its zonal extent was narrower evolving to a cyclonic pair over the eastern Pacific. Differences in circulation pattern also occur in the extratropics. The most obvious difference is the pattern orientation over the North America. The Niño3.4 index regression pattern has a north-south dipole structure, with an anti-cyclonic anomaly in the north and a cyclonic anomaly in the south, whereas in DJF 2014/15 observations the spatial pattern has an east-west dipole structure, with cyclonic anomaly in the east and anti-cyclonic anomaly in the west. From a global perspective, in both cases the pattern over the North America is part of a wave train emanating from the tropical Pacific, and thus, the causes of the difference for both the patterns may still be in the tropics.

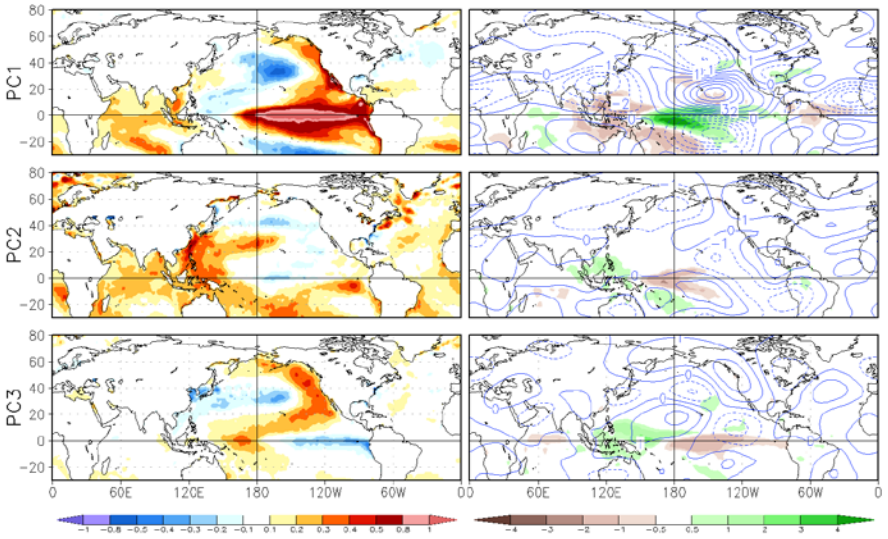

Fig. 2 Regressions of DJF mean SST (left), precipitation rate and 200hPa stream function (right) onto the first (upper), second (middle) and third (lower) principal components of the SSTs in the Pacific north of 30°S. Units are the same in Fig. 1.

The role of tropical diabatic heating (as inferred from the Prate) in influencing global circulation during ENSO winters has been demonstrated in model experiments (Hoerling and Kumar 2002 and references therein) and in diagnostic analyses (Ting and Hoerling 1993, Peng 1995, DeWeaver and Nigam 2004). The anti-cyclonic (cyclonic) pair straddling the diabatic heating (cooling) in the central equatorial Pacific has been inferred to as the forced response to the heating-cooling pair over the equatorial Pacific with the Rossby wave propagation extending this response into extratropical latitudes (Gill 1980, Sardeshmukh and Hoskins 1988). The canonical ENSO heating- circulation relationship, however, does not seem to be at play for the winter of 2014/15 as the anti-cyclonic pair, instead of associated with the heating, straddles the cooling. This leads to the question as to what drove the SST and circulation anomalies, and what was the dynamics behind the tropical circulation anomalies for 2014/15 winter?

In this study we intend to examine the effects of dominant modes of wintertime SST variability using a decomposition procedure, and then assess the relative importance of these modes through a reconstruction procedure on the observed DJF 2014/15 SST and circulation anomalies.

2. Data and analysis procedures

The data used in this study include monthly mean SST, 200hPa stream function (S200) and 1000hPa wind from Jan 1949 to Feb 2015, including 66 DJF seasons, and DJF mean precipitation from 1979/80 to 2014/15 for total 36 winters. The SST is taken from Hurrell *et al.* (2008), the stream function from NCEP/NCAR reanalysis (Kalnay *et al.* 1996), and the Prate from the CPC merged analysis of precipitation (CMAP) (Xie and Akin 1996). The anomalies of these variables are with respect to the seasonal climate mean over the respective data periods. The analysis procedure begins from an empirical orthogonal function (EOF) analysis for the 66-winter Pacific SSTs. The spatial domain for the analysis is the north of 30°S and between 120°E and 80°W, including the tropical and northern part of Pacific, same as that in Hartmann

(2015a). The EOF calculation is based on a covariance matrix such that fewer dominant modes explain more variance. After computing the principal components (PCs), which are the time series associated with EOFs, the corresponding spatial patterns of SST are obtained with the regression of the global SSTs at each grid point onto the PCs. Following the same procedure, S200 and Prate regression patterns associated with the SST modes are also obtained. As the Prate is only available from 1979, the PC time series used for regression is from that year onward.

After the decomposition procedure, the relative importance of the SST modes in explaining the observed anomalies of the three variables for DJF 2014/15 is assessed with a reconstruction procedure. The procedure starts from the most dominant mode, and then successive modes are added at each step, until a spatial pattern resembling the observed DJF 2014/15 anomalies is reconstructed. For SST, the EOF modes can completely reconstruct the observed anomalies, because they are the modes of SST itself. For S200 and Prate, however, only a part of variance can be explained by the SST EOF modes. As a result, the constructed S200 or Prate is not as accurate as that for SST.

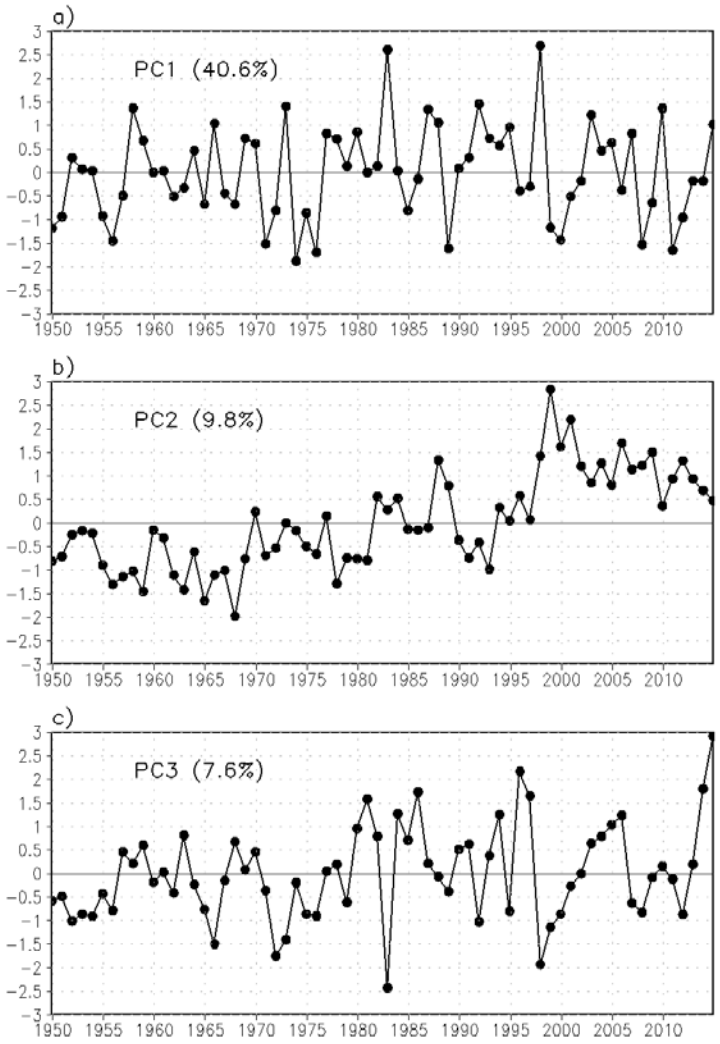

Fig. 3 Principle components (PCs) 1-3 of the DJF SSTs in the Pacific north of 30°S and percentages of their explained variance. PCs are normalized with their own standard deviation.

3. Results

Fig. 2 shows the patterns of SST, Prate and S200 associated with the first three EOF modes of SST. The corresponding PCs are displayed in Fig. 3. The first mode, explaining 41% variance of SST over the domain for the EOF analysis, is related to ENSO and referred to as ENSO mode. The SST EOF pattern and associated S200 and Prate patterns are almost identical to those from regressions with Niño 3.4 index shown in Fig. 1. The PC value of the ENSO mode for the DJF 2014/15 winter is around 1, indicating that the ENSO signal was pretty robust and was important.

The second mode, explaining about 10% variance of SST over the domain, has its major SST loading in the western and southern tropical Pacific, and also associates with anomalies in the Indian and Atlantic Oceans. The corresponding PC2 indicates that this mode is related to warming trend in the oceans, though interannual variability is also included. Its associated Prate pattern is likely a response to the SSTs with dry (wet) anomalies collocated with cold (warm) SST anomalies in the central (western) Pacific. Further, the spatial pattern of the Prate is very similar to that associated with the warm phase of ENSO, but with opposite sign and much weaker intensity. The corresponding S200 pattern in the tropics includes a cyclonic system towards the south of the negative Prate and a cross-equator system over the eastern Pacific. According to their location, shape and orientation, the former is likely forced by the diabatic cooling corresponding to the negative Prate, while the latter is more complicated. In the northern extratropics, a cyclonic system is

centered over Bering Sea and with a westward extension towards Mongolia. This mode was not part of Hartmann (2015a) analysis, because their data were detrended prior to the EOF analysis.

The third mode, explaining about 8% variance of SST over the domain, is the North Pacific Mode (NPM). The SST pattern is similar to that in Hartmann (2015a), though our analysis is based on the DJF seasonal means alone, and not the monthly means over the entire annual cycle. Its larger amplitude in the extratropics may suggest a local origin, but it also has tropical loading in the western and central equatorial Pacific. The corresponding Prate pattern matches well with the SST pattern in the tropics, with positive anomaly over the warmer SST and negative anomaly over the colder SST. Though its SST anomalies are much weaker than that in the ENSO mode, the Prate anomalies are not weak, with their amplitude reaching almost a half of that for the ENSO mode. This is because that Prate is not linearly related to SST anomaly, and is much more dependent on total SST (Hoerling et al 1997). In the S200 pattern, a wave train clearly starts from the tropical western Pacific, the area of anomalous heating, and then extends across the North Pacific to North America with a ridge along the west coast and a trough over the northeastern part of the continent. The wave train then turns southeast towards the Atlantic and finally ends at the equator near western Africa. In the tropical eastern Pacific, a cyclonic pair is associated with the diabatic cooling, suggesting that it is forced by the cooling. The time series of this mode (Fig. 3c) is dominated by interannual variability before 1998, but after that by variations on a lower frequency. The PC values were notably high for DJF 2013/14 (1.75) and 14/15 (2.90), with latter being the highest in the record analyzed.

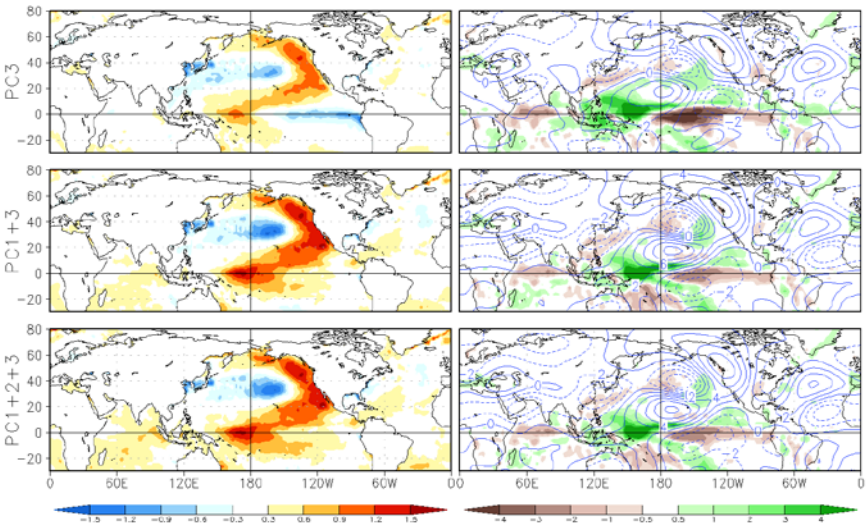

Fig. 4 Reconstructed SST (left), precipitation rate and 200hPa stream function (right) for DJF 2014/15 with spatial patterns shown in Fig. 2 and PCs shown in Fig. 3. Upper row is for using NPM alone, middle row for using both NPM and ENSO mode, and lower row for using all NPM, ENSO and warming trend modes. Unites are the same as that in Fig. 1.

The fourth mode (not shown) is the Pacific decadal oscillation (PDO) mode, which is the second mode in Hartmann 2015a. The reason for the second mode in Hartmann 2015a to be the fourth mode here may be related to the difference in data length and trend removal or not (Wen et al. 2014). The data used in Hartmann 2015 was from 1900, about 50 years longer than here. Because its PC value for DJF 2014/15 is only 0.25, its impact is small. Other SST modes are either with small PC values for DJF 2014/15 or with weak patterns. Therefore our analysis is limited to the three leading modes.

The correlation maps corresponding to the regression maps for each mode were also checked, and it is found that most features shown in Fig. 2 are well above the 90% significant level in the T-test. We also calculated the PCs and the regression patterns with the data not including 2014/15 winter and compared them with that from the full dataset as shown in Fig. 2, and found differences to be very small.

We next reconstruct the DJF 2014/15 observed anomalies based on the EOF modes. Having examined the three leading modes and noting that SST anomaly pattern for DJF 2014/15 fits best the NPM (Fig. 2, bottom left panel), the reconstruction procedure starts from the NPM. The upper row of Fig. 4 is the reconstructed SST, Prate and S200 patterns associated with the NPM, that is, the product of PC3 value for DJF 2014/15 winter and the spatial patterns associated with the EOF3 of SST shown in Fig. 2 (bottom row). Compared to the observed anomalies shown in Fig. 1 (upper row), as expected, the reconstructed SST

resembles the observation very well, particularly for the warm anomalies over the Pacific domain. However some differences are also obvious. The strong cold anomaly in the eastern equatorial Pacific is not found in the DJF 2014/15 observation, and the intensity of the reconstructed warm SST anomaly is too weak. For the Prate, the reconstructed pattern matches well the observed anomaly not only in the tropics, but also in North Pacific and North America. A major difference is in the intensity in the tropical Pacific, where the reconstructed anomaly is much stronger than the observed. For the S200, as described before, the reconstructed pattern is a wave train emanating from the diabatic heating area (correspond to the Prate) in the tropical western Pacific, with its features matching well with the observations, particularly over the North America. Major differences are that the anti-cyclonic center in the tropical central Pacific is shifted westward, and the intensity of the wave train appears weaker. Therefore, the NPM, although prominent, it alone is not adequate to explain the observed DJF 2014/15 anomalies in the tropical and North Pacific.

Because the amplitude of the ENSO mode is the strongest among all (Fig. 1) and PC1 value for DJF 2014/15 is around 1.0 for this winter, the contribution of the ENSO mode needs to be considered. The middle row of the Fig. 4 presents the reconstructed patterns after adding the ENSO mode. Comparing them with the reconstruction with the NPM alone (Fig. 4, upper row) and that from the observations (Fig. 1, upper row), we can see that the correspondence with the observed anomalies improved: (a) the cold SST anomaly in the eastern equatorial Pacific disappeared and the intensity of the warm SST anomalies increased to the level in observations; (b) the intensity of tropical Prate also reduced to the level in the observation; (c) the westward shift of the anti-cyclonic center also corrected to some extent; (d) the wave amplitude increased to that in the observation. Improvements, however, were not unanimous, for example, the trough over the northeastern part of North America became weaker, and so is the cyclonic pair in the tropical eastern Pacific.

The results of the reconstruction by adding the mode 3 are displayed in the lower row of Fig. 4. As already indicated by the mode's small PC value of 0.5 and the relatively weak circulation and precipitation patterns, the improvement is quite limited. A discernible improvement for SST is in the tropical western Pacific and India Ocean, where the SSTs became a bit warmer. Overall, the SST, precipitation and circulation anomalies in the winter of 2014/15 basically can be explained by the NPM and ENSO mode. The NPM was a dominant factor, which explains why the atmospheric anomalies did not conform to the typical ENSO response pattern (Barnston 2015).

4. Summary and discussion

In an effort to explain why the atmospheric circulation and SST anomalies of 2014/15 winter in the central equatorial Pacific lacked ocean-atmosphere coupling seen in a typical ENSO event, this study decomposed the SST, precipitation rate and 200hPa stream function anomalies for the DJF 2014/15 into the patterns related to the principal components of the DJF SST variability. We then identified the relative importance of these patterns in contributing to observed DJF 2014/15anomalies. It is found that the anomalies of the three variables were determined by the patterns related to the two SST modes, the NPM and the ENSO mode. The contribution from the NPM dominated and resulted in the seemingly uncoupled air-sea relationship in the central equatorial Pacific and the east-west structure of the observed circulation anomalies over the North America. The contribution of the ENSO mode was important for the observed SST anomalies in the eastern equatorial Pacific and for the circulation in the central equatorial Pacific. The ENSO mode was also important for the intensity of SST, precipitation rate and circulation patterns to reach the levels in the observation. The impact from the warming trend mode was found to be much small.

Acknowledgments. We would like to thank Dr. Caihong Wen for her constructive suggestions.

References

Ashok, K., S. K. Behera, S. A. Rao, H. Weng, and T. Yamagata, 2007: El Niño Modoki and its possible teleconnection. *J. Geophys. Res.*, **112**, C11007.

Barnston, T., 2015: Do recent global precipitation anomalies resemble those of El Niño? http://www.climate.gov/news-features/blogs/enso.

Bjerknes, J., 1969: Atmospheric teleconnections from the equatorial Pacific. *Mon. Wea. Rev.*, **97**, 163– 172.

DeWeaver, E., and S. Nigam, 2004: On the forcing of ENSO teleconnections by anomalous heating and cooling. *J. Climate*, **17**, 3225–3235.

Gill, A.E., 1980: Some simple solutions for heat-induced tropical circulation. *Q. J. R. Meteorol. Soc.*, **106**, 447–462.

Hartmann, D., 2015a: Pacific sea surface temperature and the winter of 2014, *Geophys. Res. Lett.*, **42**, doi:10.1002/2015GL063083.

Hartmann, D., 2015b: The tropics as a prime suspect behind the warm-cold split over North America during recent winters, http://www.climate.gov/news-features/blogs/enso.

Hoerling, M., A. Kumar, and M. Zhong, 1997: El Niño, La Niña, and the nonlinearity of their teleconnections. *J. Climate*, **10**, 1769–1786.

Hoerling, M., and A. Kumar, 2002: Atmospheric response patterns associated with tropical forcing. *J. Climate*, **15**, 2184–2203.

Hurrell, J., J. Hack, D. Shea, J. Caron, and J. Rosinski, 2008: A new sea surface temperature and sea ice boundary dataset for the community atmosphere model. *J. Climate*, **21**, 5145–5153.

Kao, H.-Y., and J.-Y. Yu, 2009: Contrasting Eastern-Pacific and Central-Pacific types of ENSO. J. Climate, **22**, 615–632.

Kalnay, E. and coauthors, 1996: The NCEP/NCAR 40-year reanalysis project. *Bull. Amer. Meteor. Soc.*, **77**, 437-471.

Peng, P., 1995: Dynamics of stationary wave anomalies associated with ENSO in the COLA GCM. Ph.D. thesis, University of Maryland, College Park, 180 pp.

Peng, P., A. Kumar, and B. Jha, 2014: Climate mean, variability and dominant patterns of the Northern Hemisphere wintertime mean atmospheric circulation in the NCEP CFSv2, *Climate Dynamics*, **42**, 2783-2799.

Sardeshmukh, P. and B. Hoskins, 1988: The generation of global rotational flow by steady idealized tropical divergence. *J. Atmos. Sci.*, **45**, 1228–1251.

Saha, S. and coauthors, 2014: The NCEP Climate Forecast System Version 2. *J. Climate*, **27**, 2185–2208.

Ting, M. and M. Hoerling, 1993: Dynamics of stationary wave anomalies during the 1986/87 El Niño. *Climate Dynamics*, **9**, 147-164.

Wen, C., A. Kumar, and Y. Xue, 2014: Factors contributing to uncertainty in Pacific Decadal Oscillation index, *Geophys. Res. Lett.*, **41**, 7980–7986, doi:10.1002/2014GL061992.

Xie, P., and P. A. Akin, 1996: Analysis of global monthly precipitation using gauge observations, satellite estimates, and Numerical model predictions. *J. Climate*, **9**, 840-858.